

Digital holography for second harmonic microscopy: application to 3D-tracking of nanoparticles

Etienne Shaffer and Christian Depeursinge

École Polytechnique Fédérale de Lausanne (EPFL), Advanced Photonics Lab (MVD),
CH-1015 Lausanne, Switzerland.

ABSTRACT

Retrieval of the amplitude and phase of electromagnetic waves made digital holographic microscopy (DHM) capable of revealing morphological details at ultrahigh resolution in the order of a few nanometers only and precisely measuring the refractive index across a sample (e.g. cell or neuron). In short, DHM added a new dimension to optical imaging, which explains why it is such an excellent instrument for metrological, but also for biological applications. We believe that DHM is, by nature, ideally suited for nonlinear microscopy. In this work, we review the advantages of DHM for nonlinear microscopy and present its application to determination of the axial position of nonlinear nanoparticles capable of second harmonic generation.

Keywords: Nonlinear microscopy, digital holography, digital holographic microscopy (DHM), second harmonic generation (SHG), nanoparticles, 3D-tracking

1. INTRODUCTION

Digital holography (DH) is a measurement technique based on an interferometric principle, thus enabling the retrieval of both the amplitude and phase of an optical field. This measurement method has been ported to the investigation of microscopic specimens by combining interferometry and microscopy in digital holographic microscopy (DHM).¹ The ability to recover the phase of a wavefront and, consequently, precise information on the optical path length traveled by the light led to many applications, ranging from metrology to biology. It made DHM capable of revealing deformations and morphological details at a nanometer-scale resolution,² and determining with high precision cell morphology³ or its refractive index distribution.⁴ Refractive index tomography was also demonstrated.⁵ All in all, by making possible quantitative phase analysis, digital holography added a new dimension to optical imaging.

Only recently was DH combined with nonlinear microscopy^{6,7} and quantitative phase directly exploited.⁸ In this work, we explain why digital holography is ideally suited for nonlinear microscopy and describe how it can be combined with nonlinear microscopy for determination of the axial position of nonlinear nanoparticles (NPs) capable of second harmonic generation.

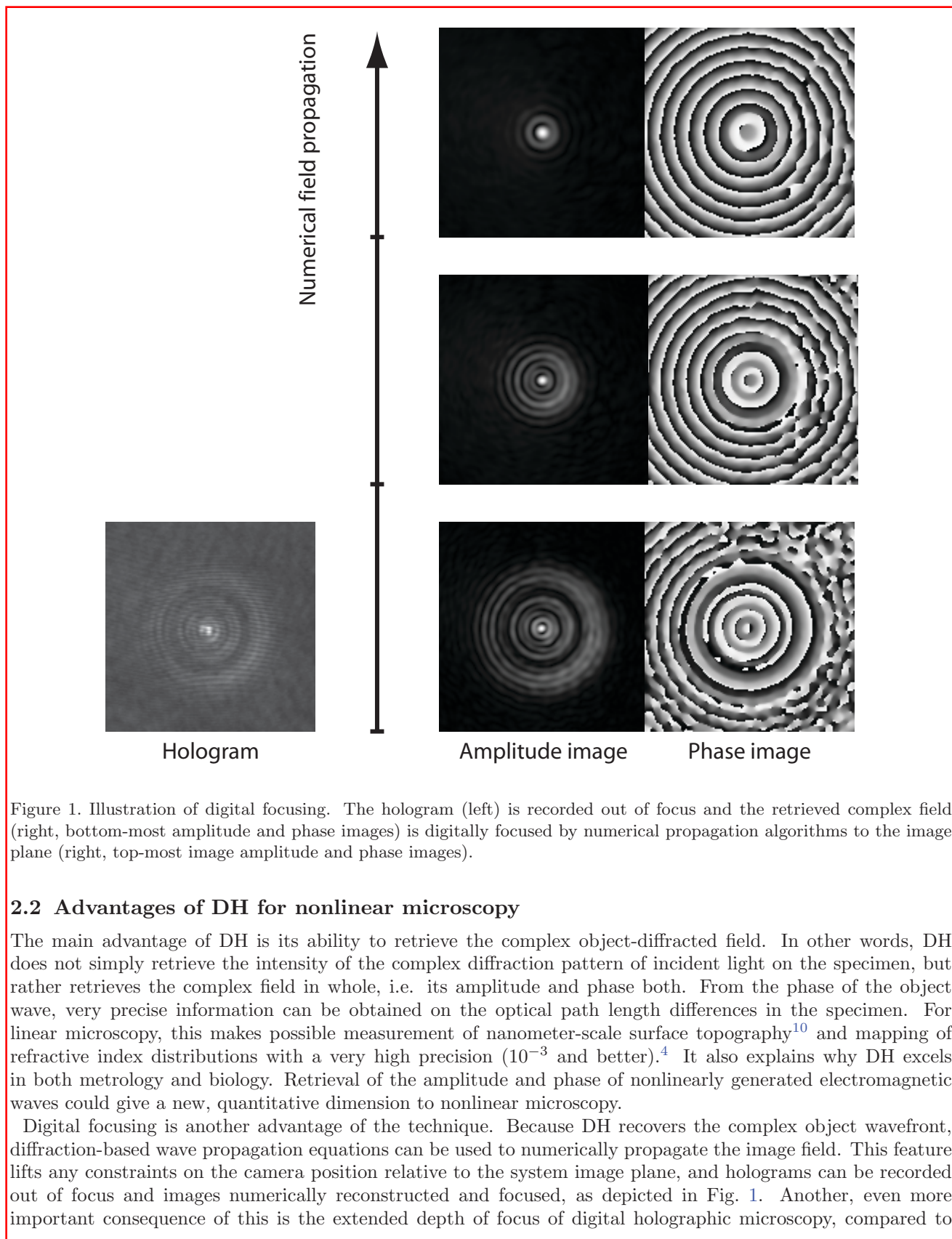
2. DIGITAL HOLOGRAPHY FOR NONLINEAR MICROSCOPY

In this section we will explain the bases of digital holography and describe its advantages for nonlinear, more specifically second harmonic, microscopy.

2.1 Digital holography basics

Holography consists in using a reference wave to encode the complex diffraction pattern of an object into an interference image called hologram. Of course, this definition assumes that the two (reference and object) waves have mutual coherence properties. Classically, holograms were recorded on a photosensitive plate and had to be photo-chemically developed and re-illuminated to produce seemingly 3D images. For the special case of digital holography (DH), holograms are recorded with a digital camera and image reconstruction is numerically performed by a computer.⁹ It is not the scope of this work to elaborate on the basis of digital holography. Details of the technique and its application to nonlinear fields can be found in Ref.⁸

E-mail: etienne.shaffer@epfl.ch



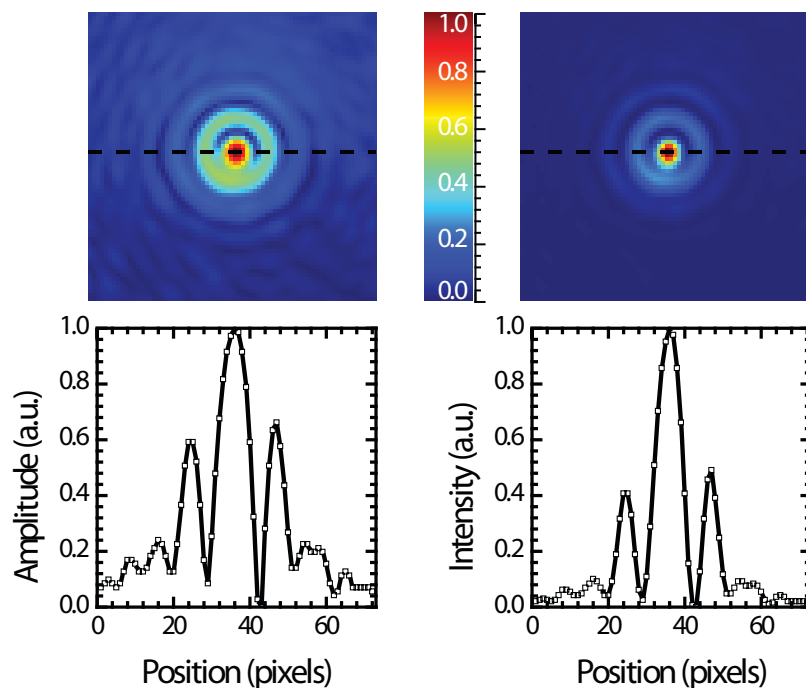


Figure 2. Comparison between amplitude and intensity type of signals. This comparison of the second harmonic signal generated by a single nanoparticle illustrates that an amplitude-based imaging technique provides a better dynamic sampling of weaker signals than an intensity-based technique.

other microscopy techniques, as objects lying outside the depth of focus of the microscope objective can still be reconstructed and numerically propagated to their respective image plane, and therefore be brought into focus.

Furthermore, because it recovers the amplitude of electromagnetic waves, DH has a better sampling of weak signals than any intensity-based imaging technique. Fig. 2 compares amplitude and intensity signals of a second harmonic emitter - from a specimen consisting of gold NPs. The dynamic range of the weaker signals is evidently higher for an amplitude-based technique. In addition, hologram can be recorded out of focus to spread the signal from a strong scatterer on many pixels, to avoid saturating the camera or compromising the dynamic range of weaker signals. Moreover, and thanks to its interferometric nature, DH benefits from coherent amplification.¹¹ This means that for a given number of photons in the object wavefront, the signal to noise ratio can be significantly increased, even doubled, simply by increasing the number of photons in the reference wavefront. This is extremely important for nonlinear signals, like SHG, that are generally of relatively low intensities. Finally, off-axis DH is a full-field, single shot acquisition technique. Since it requires no scanning whatsoever, it is very fast (real-time acquisition and processing) and insensitive to vibrations, for relatively small camera shutter times.

3. APPLICATION TO 3D-TRACKING OF NANOPARTICLES

Nanoparticles are now commonly used in biology as labels or contrast agents for imaging¹² and for detection of specific pathogens or proteins.¹³ In addition, they appear very promising for bottom-up tissue engineering,¹⁴ for drug or gene delivery^{15,16} to specific cellular sites and even for tumor treatment.¹⁷ Gold nanoparticles, in particular, have been extensively investigated because of their excellent bio-compatibility and chemically inert nature, and nowadays a vast knowledge on how to functionalize gold nanoparticles has been developed. Be it for micro-fluidic or targeted biomedical applications, precise real-time 3D-tracking of nanoparticles is becoming an urgent need to fill. Over the years, many methods¹⁸⁻²⁴ were developed for determination the lateral position of NPs from optical images, presumably at nanometer (or at least sub-pixel) resolution, although one must be very careful with such claims. These methods are mostly based on post-processing and analyses of optical images,

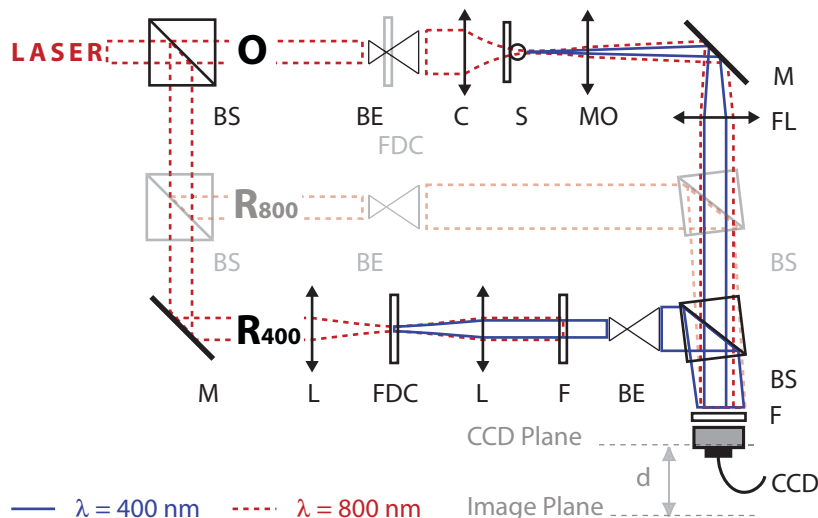


Figure 3. Experimental setup schematics: *BS* beamsplitter, *BE* beam expander, *C* condenser lens, *S* specimen, *MO* 100× microscope objective, *M* mirror, *FL* field lens, *F* filter, *L* lens and *FDC* frequency doubler crystal. **O** designates the object arm, while **R₈₀₀** and **R₄₀₀** respectively designate the reference arms for the fundamental and second harmonic wavelengths.

by cross-correlation,¹⁸ sum-absolute difference,¹⁹ centroid,²⁰ direct Gaussian fit^{21,22} or polynomial-fit Gaussian-weight.²³ A comparative study of these methods is proposed in Ref.²⁴ The real challenge to 3D-tracking always has been and remains the determination of the axial position, which is no better than the 10-100 micrometer range, unless the complex diffraction field can be accessed. Even then, it does not reach far below the sub-micrometer without *a priori* knowledge of shape or size of the particle.

Here, we focus on determination of the axial position, a challenge we address by numerical focusing of the complex second harmonic field, retrieved with digital holography. It should be emphasized that the described holographic technique is compatible with previously-cited methods for determination of lateral position.

3.1 Experimental details

Schematics of the optical setup used for experiments can be found in Fig 3. The laser source is a 800 nm wavelength Ti:Sapphire laser delivering 250 fs pulses at approximately 250 kHz repetition rate. In the object arm **O** of our Mach-Zehnder type interferometric setup, light is focused in the specimen plane by a *f*/4 aperture condenser lens and then collected by a 100× microscope objective. A β -barium borate (BBO) frequency doubler crystal (FDC) is inserted in the reference arm **R** to generate the second harmonic reference wave. Holograms were recorded using a -20°C -cooled CCD camera (12-bits) and a 400 ± 20 nm bandpass filter eliminates the fundamental-wavelength component of light. The laser peak power in the specimen plane is of approximately $30 \text{ GW}\cdot\text{cm}^{-2}\cdot\text{pulse}^{-1}$, which is about one order of magnitude below the threshold for biological cell damage,²⁵ and could potentially be reduced by the use of a more sensitive camera, e.g. EMCCD-type, or more efficient NPs.

To demonstrate the ability of the proposed technique to 3D-tracking of nanoparticles, we have mounted the specimen on a feedback-looped piezoelectric stage, with a sub-nanometer resolution. The studied specimen consists of a solution of BaTiO₃ nanoparticles of tetragonal crystalline structure and of relatively large mean size (200 nm) deposited on a glass coverslip. During the experiment, the specimen was axially scanned over a range of 2 micrometers, with a sampling step of 25 nm. Eight holograms were recorded at every position for statistic analysis of the efficiency of each technique.

It is very important to emphasize that digital holography, as proposed here, is a single-shot technique. This means that a single hologram acquisition leads to complex wavefront retrieval over the entire field of view. As a consequence, the technique is said to be vibration-insensitive, in opposition to scanning microscopy techniques.

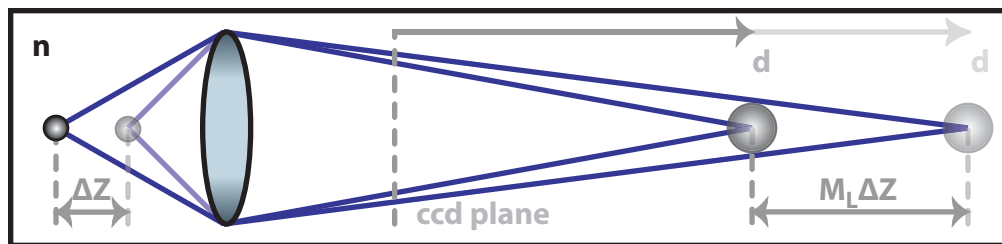


Figure 4. Cartoon depicting how the position of the image plane, and thus the reconstruction distance d required to bring the complex second harmonic field to focus, depends on the axial position of the emitter. If the nanoparticle is moved along the optical axis by ΔZ in the object space, its image plane will shift by $M_L \Delta Z$ in the image space, where M_L is the longitudinal magnification of the system.

However, this is no longer the case when comparing the reconstructed fields from different holograms, as the absolute phase may have been arbitrarily shifted between the two acquisitions. In classical, i.e. linear, digital holography, this problem is easily overcome by referencing the phase variations of the specimen (e.g. a cell) to the phase offset in a region of the background where the phase is expected to remain unchanged (e.g. the coverslip). Unfortunately, this is not possible with a background-free technique, such as the one presented here, where the only collected SHG signal comes from the specimen. To produce a uniform, unvarying SHG background on which to reference the phase variations and eliminate those attributed to system vibrations, we have installed a lithium triborate (LBO) crystal — indicated by FDC in Fig. 1 — in the focal plane of the beam expander located in the object arm of the interferometer. Referencing the SHG phase from the specimen to that of the LBO-generated background cancels out almost all vibrations-induced phase variations. Even so, phase variations caused by vibrations between the LBO crystal and the specimen remain, because they introduce a different phase shift for the fundamental (that will generate the SHG at the specimen) and the second harmonic (generated by the LBO crystal) wavelengths. The remaining phase variations account for approximately 5% of the overall phase noise.

3.2 Method for axial position determination

The method we propose for determining the relative z -position of SHG point-source emitters is based on numerical propagation of the SHG field recovered from hologram processing, as described in Ref.⁹ and detailed for second harmonic generation in Ref.⁸ The idea is that the intensity of the second harmonic field generated by a NP will reach a maximum at an axial position corresponding to the image plane. Then, the exact position of the image plane (in the image space) can be related to the axial position of that NP (in the object space), as depicted in Fig. 4. In other words, the reconstruction distance d between the hologram plane and the image plane depends on the axial position of the SHG emitter, and it is possible to deduce the relative axial positions (in the object space) of different SHG emitters from the reconstruction distances that maximize their respective SHG field intensity (in the image space). The resolution of this method strongly depends on the precision at which the reconstruction distance can be determined. Ultimately, the axial resolution depends on the longitudinal magnification (M_L) of the microscope objective, which, under some approximation, can be related to its transverse magnification (M_T) by

$$M_L = M_T^2. \quad (1)$$

For a $100\times$ microscope objective, a variation of $1 \mu\text{m}$ of the axial position of the SHG emitter in the object space would correspond to a variation of 1 cm of the reconstruction distance in the image space.

3.3 Results

We have tested this method on the stack of holograms we have recorded according to the protocol described in Section 3.1. For each of the 640 holograms (i.e. 8 holograms at each of the eighty 25 nm steps) the phase of the constant SHG background generated by the BBO crystal in the object arm (see Fig. 1) was set to zero, to eliminate the nefast effects of vibrations in the system (see Section 3.1). Each hologram was processed independently. An

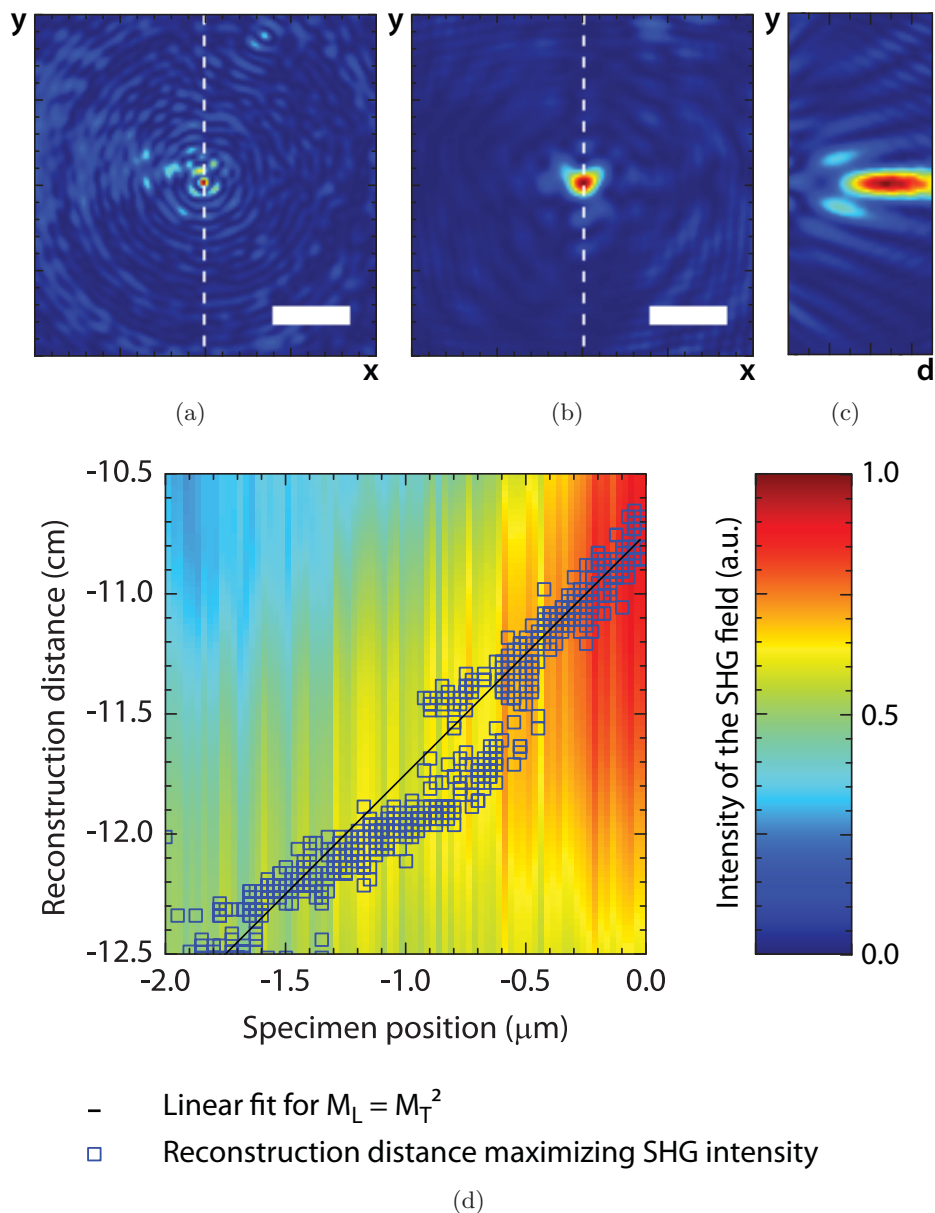


Figure 5. Second harmonic generation (SHG) by a nanoparticle. (a) and (b) Transverse (xy) cross-section of the intensity of the SHG field, respectively in the hologram plane and after hologram reconstruction in the image plane. Scale bars are 2 microns. (c) Intensity of the SHG field along the dashed white line trace in (a) and (b) for hologram reconstruction distances (d) varying between -8 and -15 cm. (d) Color-coded in jet is the maximum SHG field intensity vs reconstruction distance, for different axial positions of the specimen, when scanned with a piezoelectric stage. Blue squares indicates the reconstruction distance maximizing the SHG field intensity and black line represents the linear fit of Eq. (1).

automatic procedure was used for hologram reconstruction and optimization of the reconstruction distance was based on maximization of the SHG intensity.

Typical reconstructed SHG field intensity in the hologram plane and after numerical propagation to the image plane are respectively displayed in Fig. 5(a) and 5(b). Fig. 5(c) maps the intensity along the white line present in the two previous images, for reconstruction distances varying between -15 and -8 cm. For every specimen position and reconstruction distance, the intensity of the brightest pixel is color-coded in the background of the graph of Fig. 5(d), where the optimized reconstruction distance is plotted against the axial position returned by the piezoelectric stage. The graph shows an overall linear relation between axial position of the specimen in the object space and reconstruction distance (or axial position of the image plane) in the image space. It should be noted that the objective working distance more or less corresponds to the $0 \mu\text{m}$ axial position in the graph, where the slope is more regular and, as expected from Eq. (1), corresponds to M_T^2 — plotted in black line. For our $100\times$ objective, moving the specimen by $1 \mu\text{m}$ causes the reconstruction distance to change by 1 cm. While the reconstruction distance can theoretically be infinitely small, the real resolution limit is imposed by experimental conditions. But as the specimen moves too far away from the working distance, aberrations disrupt the linear relation. From the graph of Fig. 5(d), we evaluate the axial resolution of this method to be a few hundreds of nanometers, for positions close to the working distance. This is one order of magnitude better than initially estimated by Hsieh *et al.*⁷

3.4 Summary

We evaluate the axial resolution of this method to be roughly 200-400 nm, which compares to Ref.²⁶ and is much better than many other optical tracking techniques, but still not as high as one would expect from an interferometric technique. Because this method is based on an imaging scheme, it is very much dependent on geometrical configuration and optical aberrations, which is a major disadvantage. Indeed, for a specimen lying far from the optical axis or the objective working distance, the relation between the reconstruction distance and the real position of the specimen no longer follows Eq. (1). In any cases, that relation is a rough approximation and is not expected to remain valid for non-ideal imaging conditions. Unfortunately, this method is extremely time-consuming, therefore incompatible with real-time imaging, since after the complex field is recovered from each hologram, an optimization routine is needed for determination of the reconstruction distance that maximizes the intensity of the SHG field. In digital holography, numerical field propagation is the step requiring the most processing time and optimization routines roughly require to perform between 10 and 100 of these numerical propagation steps. It is therefore doubtful that this method reaches real-time processing. However, as hologram recording is only limited in speed by the detector frame rate, a stack of holograms could be recorded live and processed later to retrieve the axial positions of the nanoparticles.

4. CONCLUSION

In conclusion, we have presented the advantages that digital holography offers to nonlinear microscopy, among which are the better sampling of weak signals, the coherent amplification and the digital focusing, but also, and more importantly, the complex field retrieval, which leads to, among the many possibilities digital holography offer to nonlinear microscopy, 3D-tracking of nanoparticles. With this technique, axial resolutions of 200-400 nm can be obtained from hologram processing. Furthermore, the technique can be straightforwardly adapted to other nonlinear fields, such as third harmonic generation, sum- or difference-frequency, or coherent anti-Stokes Raman scattering. Finally, we believe that it has a bright future in biomedical imaging, for monitoring of targeted receptors, with use of bio-conjugated nanoparticles.

This work was financially supported in part by the Swiss National Competence Center in Biomedical Imaging (NCCBI) and by the Swiss National Science Foundation (SNSF), grant #205320-120118.

REFERENCES

- [1] Cuche, E., Bevilacqua, F., and Depeursinge, C., “Digital holography for quantitative phase-contrast imaging,” *Optics Letters* **24**, 291–293 (Mar. 1999).

- [2] Kühn, J., Charrière, F., Colomb, T., Cuche, E., Montfort, F., Emery, Y., Marquet, P., and Depeursinge, C., "Axial sub-nanometer accuracy in digital holographic microscopy," *Measurement Science and Technology* **19**, 074007 (2008). citation group.
- [3] Rappaz, B., Charrière, F., Depeursinge, C., Magistretti, P. J., and Marquet, P., "Simultaneous cell morphometry and refractive index measurement with dual-wavelength digital holographic microscopy and dye-enhanced dispersion of perfusion medium," *Optics Letters* **33**(7), 744–746 (2008). citation group.
- [4] Marquet, P., Rappaz, B., Magistretti, P. J., Cuche, E., Emery, Y., Colomb, T., and Depeursinge, C., "Digital holographic microscopy: a noninvasive contrast imaging technique allowing quantitative visualization of living cells with subwavelength axial accuracy," *Optics Letters* **30**(5), 468–470 (2005). citation group.
- [5] Charrière, F., Marian, A., Montfort, F., Kühn, J., Colomb, T., Cuche, E., Marquet, P., and Depeursinge, C., "Cell refractive index tomography by digital holographic microscopy," *Optics Letters* **31**(2), 178–180 (2006). citation group.
- [6] Pu, Y., Centurion, M., and Psaltis, D., "Harmonic holography: a new holographic principle," *Applied Optics* **47**, A103–A110 (Feb. 2008).
- [7] Hsieh, C.-L., Grange, R., Pu, Y., and Psaltis, D., "Three-dimensional harmonic holographic microscopy using nanoparticles as probes for cell imaging," *Opt. Express* **17**, 2880–2891 (Feb. 2009).
- [8] Shaffer, E., Pavillon, N., Kühn, J., and Depeursinge, C., "Digital holographic microscopy investigation of second harmonic generated at a glass/air interface," *Optics Letters* **34**, 2450–2452 (Aug. 2009).
- [9] Schnars, U. and Jüptner, W. P. O., "Digital recording and numerical reconstruction of holograms," *Measurement Science & Technology* **13**, R85–R101 (Sept. 2002).
- [10] Kühn, J., Montfort, F., Colomb, T., Rappaz, B., Moratal, C., Pavillon, N., Marquet, P., and Depeursinge, C., "Submicrometer tomography of cells by multiple-wavelength digital holographic microscopy in reflection," *Optics Letters* **34**, 653–655 (Mar. 2009).
- [11] Charrière, F., Colomb, T., Montfort, F., Cuche, E., Marquet, P., and Depeursinge, C., "Shot noise influence in reconstructed phase image snr in digital holographic microscopy," *Applied Optics* **45**(29), 7667–7673 (2006). citation group.
- [12] Thurn, K. T., Brown, E. M. B., Wu, A., Vogt, S., Lai, B., Maser, J., Paunesku, T., and Woloschak, G. E., "Nanoparticles for applications in cellular imaging," *Nanoscale Research Letters* **2**, 430–441 (Sept. 2007).
- [13] Gu, H. W., Xu, K. M., Xu, C. J., and Xu, B., "Biofunctional magnetic nanoparticles for protein separation and pathogen detection," *Chemical Communications* **37**(9), 941–949 (2006).
- [14] Kim, K. and Fisher, J. P., "Nanoparticle technology in bone tissue engineering," *Journal of Drug Targeting* **15**(4), 241–252 (2007).
- [15] Panyam, J. and Labhasetwar, V., "Biodegradable nanoparticles for drug and gene delivery to cells and tissue," *Advanced Drug Delivery Reviews* **55**, 329–347 (Feb. 2003).
- [16] De Jong, W. H. and Borm, P. J. A., "Drug delivery and nanoparticles: Applications and hazards," *International Journal of Nanomedicine* **3**(2), 133–149 (2008).
- [17] Day, E. S., Morton, J. G., and West, J. L., "Nanoparticles for thermal cancer therapy," *Journal of Biomechanical Engineering-transactions of the Asme* **131**, 074001 (July 2009).
- [18] Gelles, J., Schnapp, B. J., and Sheetz, M. P., "Tracking kinesin-driven movements with nanometer-scale precision," *Nature* **331**, 450–453 (Feb. 1988).
- [19] Bohs, L. N., Geiman, B. J., Anderson, M. E., Gebhart, S. C., and Trahey, G. E., "Speckle tracking for multi-dimensional flow estimation," *Ultrasonics* **38**, 369–375 (Mar. 2000).
- [20] Ghosh, R. N. and Webb, W. W., "Automated detection and tracking of individual and clustered cell surface low density lipoprotein receptor," *Biophysical Journal* **66**, 1301–1318 (May 1994).
- [21] Anderson, C. M., Georgiou, G. N., Morrison, I. E. G., Stevenson, G. V. W., and Cherry, R. J., "Tracking of cell surface receptors by fluorescence digital imaging microscopy using a charge-coupled device - low-density-lipoprotein and influenza-virus receptor mobility at 4 degrees c," *Journal of Cell Science* **101**, 415–425 (Feb. 1992).
- [22] Schutz, G. J., Schindler, H., and Schmidt, T., "Single-molecule microscopy on model membranes reveals anomalous diffusion," *Biophysical Journal* **73**, 1073–1080 (Aug. 1997).

- [23] Rogers, S. S., Waigh, T. A., Zhao, X. B., and Lu, J. R., "Precise particle tracking against a complicated background: polynomial fitting with gaussian weight," *Physical Biology* **4**, 220–227 (Sept. 2007).
- [24] Cheezum, M. K., Walker, W. F., and Guilford, W. H., "Quantitative comparison of algorithms for tracking single fluorescent particles," *Biophysical Journal* **81**, 2378–2388 (Oct. 2001).
- [25] Konig, K., So, P. T. C., Mantulin, W. W., and Gratton, E., "Cellular response to near-infrared femtosecond laser pulses in two-photon microscopes," *Optics Letters* **22**, 135–136 (Jan. 1997).
- [26] Atlan, M., Gross, M., Desbiolles, P., Absil, E., Tessier, G., and Coppey-Moisan, M., "Heterodyne holographic microscopy of gold particles," *Optics Letters* **33**, 500–502 (Mar. 2008).